Bangladesh Journal of Physics, Vol. ***29****, Issue 1, pp. 13 – 24, June 2022*

STUDY THE INFLUENCE OF ANNEALING TEMPERATURE ON THE STRUCTURAL CHARACTERISTICS OF $Fe_{73.5-X}Cr_XCu_1Nb_3Si_{13.5}B_9$

M. M. RANA[1,6], M. R. HASSAN[2], M. H. REZVI[3,7], A. Z. ZIAUDDIN AHMED[4*], SADIA AFRIN[4], M. N. I. KHAN[5], S. MANJURA HOQUE[5], G. M. BHUIYAN[6], M. A. HAKIM[7]

[1]Department of Physics, Mohammadpur Kendriya College, Dhaka-1207, Bangladesh
[2]Rooppur Nuclear Power Plant, Pabna, Bangladesh
[3]North Carolina State University, USA
[4]Department of Basic Science, Primeasia University, Banani, Dhaka-1213, Bangladesh
[5]Material Science Division, Atomic Energy Centre, Dhaka-1000, Bangladesh
[6]Depaerment of Theoretical Physics, University of Dhaka, Dhaka-1000, Bangladesh
[7]Depaerment of Glass and Ceramic Engineering, Bangladesh University of Engineering and Technology, Dhaka-1000, Bangladesh

**Corresponding author e-mail: azzahmed@primeasia.edu.bd*
Received on 13.04.2022, Revised received on 20.05.2022, Accepted for publication on 21.05.2022

DOI: https://doi.org/10.3126/bjphy.v29i1.78685

ABSTRACT

Alloy ribbons with the composition $Fe_{73.5-x}Cr_xCu_1Nb_3Si_{13.5}B_9$ (where x = 1, 5, 10, 12.5, 17.5) are produced using a rapid quenching technique and subsequently annealed at various temperatures. The development of a homogeneous, ultra-fine grain structure, and also confirmation of the Fe(Si) phase, are examined through X-ray diffraction analysis. As the temperature increases, the amorphous nature of the as-prepared ribbons begins to diminish due to the onset of crystallization nucleation. Differential Scanning Calorimetry (DSC) measurements clearly show that the crystallization temperature shifts to higher values with increasing heating rates and time. A strong correlation between the onset of crystallization and the volume fraction of the crystalline α-Fe(Si) phase is observed through differential thermal scanning calorimetry. Additionally, Field Emission Scanning Electron Microscopy (FESEM) is employed to capture micrographs at different annealing temperatures, reflecting variations in the Cr content.

Kye Words: *Amorphous ribbon, Fe(Si) Phase, XRD, DSC, FESEM*

1. INTRODUCTION

Technological advancements in soft magnetic alloys for use in electronics, magnetic devices, and power electrical appliances have spurred growing interest in the research of Finemet alloys. Fe-Si-B-based Finemet alloys possess outstanding soft magnetic properties, making them highly suitable for high-frequency ferrite applications [1]. Researchers have discovered that Fe-Si-B alloys exhibit high saturation magnetization and low coercivity, making them promising materials for industrial applications. In the power electronics sector, nanocrystalline materials outperform other alloys, following the same trends as ferrite and amorphous materials in these applications [2, 3, 4]. During heat treatment, phase transformations in Fe-Si-B alloys, caused by microstructural evolution, significantly influence their thermal and magnetic properties [5]. The soft magnetic properties of these materials are particularly advantageous, despite their mechanical properties. The exploration

of alternative energy sources is further encouraged by the versatile applications soft magnetic Finemet alloys of Fe-Si-B [5].

The melt spinning technique, combined with thermal annealing near the crystallization temperature, is widely used to achieve desirable properties of soft magnetic materials [6]. For Fe-Si-B alloys, crystallization occurs above 510°C, and ultra-fine α-Fe(Si) grains, measuring approximately 10-20 nm, begin to grow [6]. The crystallization kinetics of Fe-Si-B-based alloys are extensively studied due to the significant phase changes that occur during heat treatment [7]. In this scientific report, the influence of heat treatment on the structural properties of alloys with varying Cr content are investigated. The study shows that increase of Cr contents improves the magnetic properties of Fe-based amorphous alloys [8]. It is also well-established that substitution of Cr in the Fe-Si-B-based amorphous alloys improves glass-forming ability and also enhancing the mechanical properties [9]. The Structural properties of $Fe_{73.5-x}Cr_xCu_1Nb3Si_{13.5}B_9$ (where x = 1, 5, 10, 12.5, and 17.5) were analyzed by X-ray diffraction (XRD) and micrographs are obtained from Field Emission Scanning Electron Microscopy (FESEM), while crystallization kinetics are studied using differential scanning calorimetry (DSC) thermographs.

2. EXPERIMENTAL

Amorphous ribbons with the composition $Fe_{73.5-x}Cr_xCu_1Nb_3Si_{13.5}B_9$ were produced using the melt-spinning technique on single-roller equipment at the Laboratory of Amorphous Materials at Hanoi University of Technology. The raw materials used, with high purity levels: Fe (99.98%), Cu (99+%), Cr (99.5%), B (99.5%), and Si (99.9%) were sourced from Johnson Matthey (Alfa Aesar). The constituent elements were accurately weighed, then melted in an arc furnace to form alloy balls. These alloy balls were subsequently placed in a quartz tube crucible for re-melting in an induction furnace under an argon atmosphere at a pressure of 10^{-6} mbar. The quartz crucible's bottom was equipped with a rectangular nozzle tip measuring 8 mm in length and 0.7 mm in width. The nozzle tip's position is adjustable relative to the copper wheel surface, enabling the molten alloy to be ejected perpendicularly onto the wheel from an approximate distance of 0.3 mm.

The molten metal was ejected using 250 mbar of overpressure by 99.9% of pure argon, supplied from an external reservoir, through the nozzle onto the surface of a rotating copper wheel having a linear velocity of 30 m/s. The thickness and the width of prepared ribbon samples are found to be approximately 20-22 μm and 6 mm respectively. Phase transitions were analyzed using thermographs generated by DSC (2960 SDT, USA). Cu-Kα radiation (wavelength: 1.54 Å) from X'Pert Pro X-ray Diffractometer (manufactured by Philips) has been used for structural characterization of the ribbons. The Field Emission Scanning Electron Microscope (FESEM, JEOL JSM 7600F) has been deployed to study the morphology of the synthesized powders. This experiment was performed at the Department of Glass and Ceramic Engineering, Bangladesh University of Engineering and Technology.

3. RESULT AND DISCUSSIONS

3.1 Crystallization Phase Analysis by Differential Scanning Calorimetry

The crystallization kinetics of various crystalline phases in $Fe_{73.5-x}Cr_xCu_1Nb_3Si_{13.5}B_9$ ribbons are examined by using DSC. Figure 1 depicted the scanned results obtained from DSC under condition of nitrogen atmosphere, at continuous heating rate 20°C/min. The exothermic peaks are displayed in

the curves, where the crystallization of α-Fe(Si) phase represented by the first peak, while Fe-B phase is represented by the second peak. It has been observed that crystallization of these phases initiated over a broad range temperature, with peak shifting towards higher temperatures region as the Cr content increased.

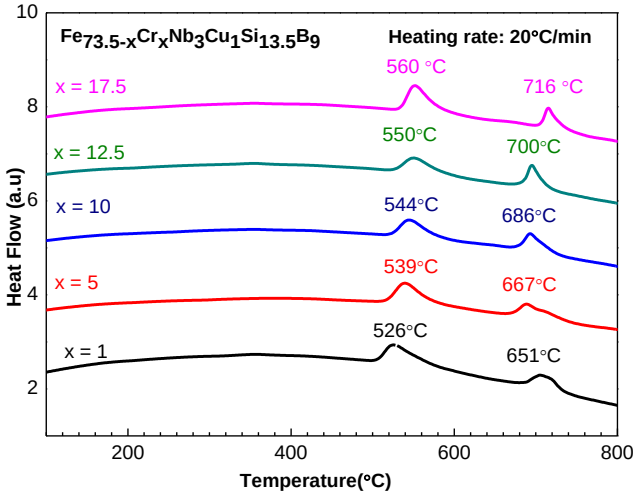

Fig. 1: Results of DSC thermograms for amorphous ribbons of $Fe_{73.5-x}Cr_xCu_1Nb_3Si_{13.5}B_9$ Finemet alloys.

This shift in crystallization peak temperatures with increase of Cr content highlights the enhanced thermal stability of the alloys after substitution of Cr-content. The two distinct exothermic peaks correspond to different crystallization events, occurring at temperatures denoted as T_{p1} and T_{p2}, respectively. Crystallization begins at temperatures where the exothermic heat flow starts to raise. The soft magnetic behavior are associated with the initial crystallization event (T_{x1}), which continues until reaching the maximum peak of α-Fe(Si) nanograin formation. The secondary crystallization (T_{x2}), associated with the Fe-B phase, results in magnetic hardening of the nano-crystalline alloys. The onset temperatures of first and second crystallization (T_{x1} and T_{x2}) and the corresponding peak temperatures (T_{p1} and T_{p2}) exhibit exothermic behavior, releasing heat at the time of crystallization of both Fe(Si) and Fe-B phases.

Table 1: Primary and secondary crystallization temperatures of $Fe_{73.5-x}Cr_xCu_1Nb_3Si_{13.5}B_9$ for x = 1, 5, 10, 12.5 and 17.5.

Cr (x)	Heating rate /min	Primary crystallization onset temperature T_{x1} in ºC	Primary peak temperature T_{p1} in ºC	Secondary crystallization onset temperature T_{x2} in ºC	Secondary peak temperature T_{p2} in ºC
1	20 ºC	494	526	640	651
5		509	539	652	667
10		514	544	667	686
12.5		517	550	675	700
17.5		524	560	698	716

3.2 X-ray Diffraction Analysis of $Fe_{73.5-x}Cr_xNb_3Cu_1Si_{13.5}B_9$

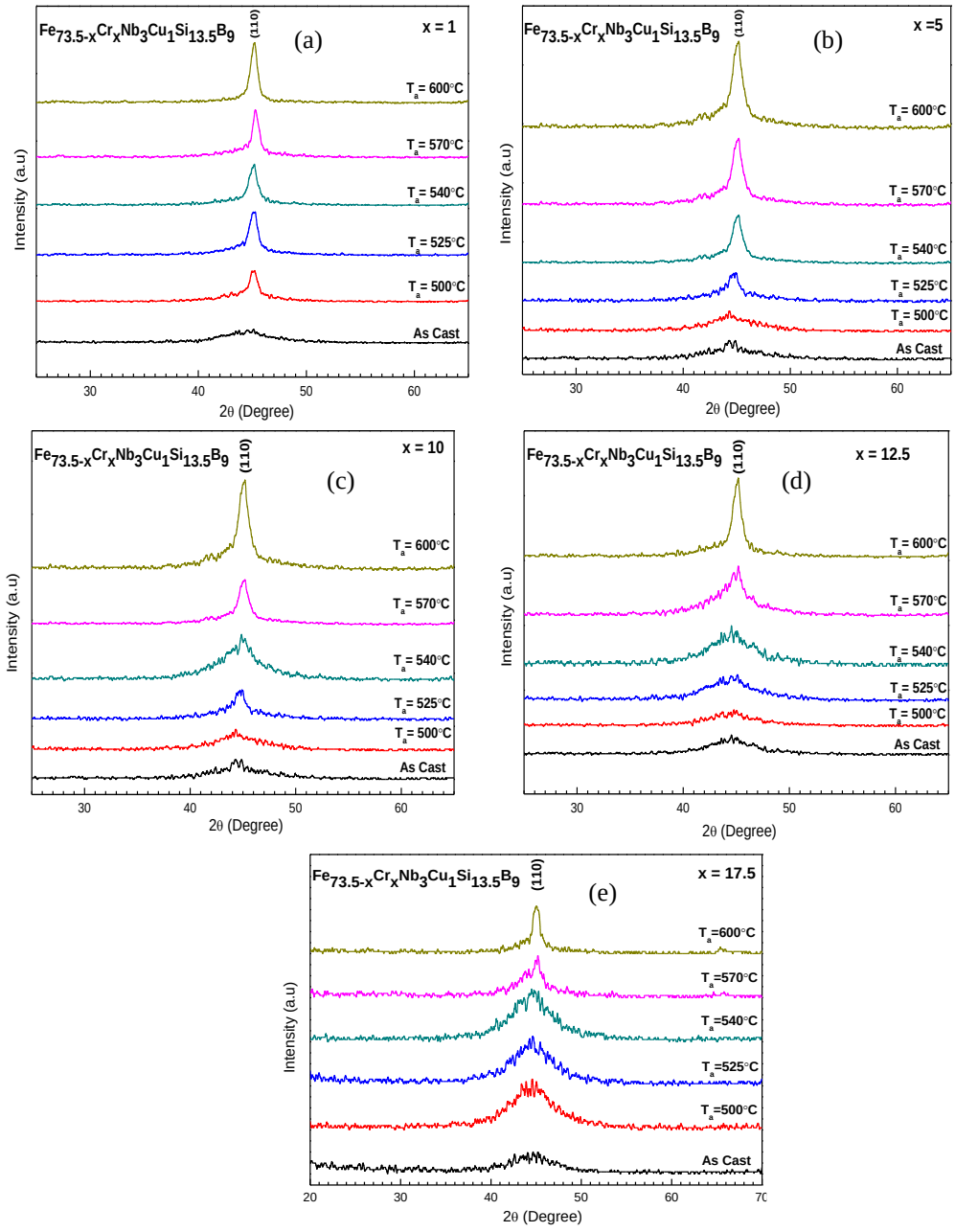

Fig. 2: XRD pattern at different annealing temperature of $Fe_{73.5-x}Cr_xNb_3Cu_1Si_{13.5}B_9$ alloys for (a) x = 1, (b) x = 5, (c) x = 10, (d) x = 12.5, (e) x = 17.5

The $Fe_{73.5-x}Cr_xNb_3Cu_1Si_{13.5}B_9$ alloys (with x = 1, 5, 10, 12.5, and 17.5) synthesized for this study has been confirmed to be amorphous structure. As illustrated in Figure 2, all samples in the series under study display humps around the angle 2θ = 45°, extending up to 10°. These diffuse humps carrier a distinct confirmation of the amorphous structure of all the as-cast samples [10, 11]. Figure 2 also presents the XRD patterns for the sample for x = 1 that annealed at various temperatures, as determined by the DSC thermogram results. The as-cast sample remains amorphous and different degrees of crystallization are observed after annealed the samples between thermodynamic state 500°C and 600°C. The sharpness and intensity of the XRD peaks increase. As the annealing temperature (T_a) increases, and when the patterns start to be narrower, shows the indication of growth of nanograins with the increase of T_a [12].

Crystallization was observed to initiate at temperatures as low as 500°C, as indicated by the DSC analysis, where the crystallization peak temperature is 526°C for the sample x = 1 is and the temperature for onset is near about 500°C. This suggests that crystallization initiated much earlier than it reached to the peak temperature, T_{p1}, near onset of primary crystallization at thermodynamic state, $T_{x1} \approx$ 594°C, as found in the DSC thermogram. The data presented in Tables 1 and Figure 2 for XRD are well aligned with the DSC results. Crystallization becomes more pronounced at T_a = 540°C and higher, as clearly shown in the XRD patterns in Figure 2. The samples having higher amount of Cr element (x = 5, 10, 12.5, and 17.5), the XRD patterns (Figures 2 (b), (c), (d), and (e)) reveal that the gradual initiation of crystallization start at temperatures less than the peak temperature (T_{p1}) and it became fully developed at higher annealing temperatures, T_a. All presented XRD patterns evidently shows that the crystallization onset certainly slow down with increasing amount of Cr element. Due to the outgrowth of annealing temperature, T_a, the total areas covered under the peak of the XRD patterns withered and become sharper, which is pointing to the growth of nanograins [13].

The crystallization process progress become very sluggish and negligible for the samples having x = 12.5 and 17.5 until temperature, T_a rises to 570°C. This establishes the enhancement of the thermal stability for increasing amount of higher element Cr, which tends to suppress the processes of crystallization [14]. Notably, even at T_a = 600°C, the crystallization in the x = 17.5 sample is not fully complete, as indicated by the nature of spread peaks. The through investigates of the peaks suggests that the phase correspond to the bcc α-Fe(Si) structure. The grain size, estimated using the formula proposed by Scherrer's [15]:

$$D_g = \frac{0.9\lambda}{\beta cos\theta}$$

Where, λ = 1.54178 Å for X-ray obtained from Cu-Kα radiation while β stands for the full width at half maximum (FWHM). The grain size at different annealing temperatures, T_a is presented in Table 2. The results show that grain size varies significantly with both annealing temperature and Cr content. It is evident from Table 2, that rise of the amount of Cr element in the FINEMET alloy leads to a significant decrease in grain size, while higher annealing temperatures tends to promote grain growth. The crystallization process is slacked down for the samples with higher Cr content, eventually which tends to keep grain sizes smaller [16].

For the x = 1 sample, the grain size reaches 10 nm at T_a reached to 500°C, while for the sample x = 5, it is increased to 11 nm at T_a = 540°C. However, no grains are detected for samples x = 12.5 and 17.5, at T_a = 540°C, suggesting that the thermal energy is insufficient to trigger crystallization at this temperature state. The distinct crystallization is observed at T_a = 600°C only, which highlights the

grain growth suppressing effect and thermal stability enhanced due to the addition of Cr content. For the samples having higher Cr-content, the XRD patterns does not found to be well-defined, so the calculations of grain size from Scherrer's formula gives an approximate result. The large amount of refractory Cr metal in these samples significantly alters the intrinsic crystallization behavior of the amorphous precursor ribbons, leading to heterogeneous crystallization as confirmed in [17].

Table 2: Grain size calculated from the XRD data of $Fe_{73.5-x}Cr_xNb_3Cu_1Si_{13.5}B_9$ crystalline alloys with different amount of Cr element and annealing temperature.

Content Cr(x)	Annealing temperature, T_a (^oC)	Crystalline Phase	Grain size (nm)
1	As cast	Amorphous	-
	500	α-Fe(Si)	10
	525	α-Fe(Si)	12
	540	α-Fe(Si)	15
	570	α-Fe(Si)	17
	600	α-Fe(Si)	20
5	As cast	Amorphous	-
	500	Amorphous	-
	525	α-Fe(Si)	4
	540	α-Fe(Si)	11
	570	α-Fe(Si)	13
	600	α-Fe(Si)	18
10	As cast	Amorphous	-
	500	Amorphous	-
	525	Amorphous	-
	540	α-Fe(Si)	4
	570	α-Fe(Si)	12
	600	α-Fe(Si)	18
12.5	As cast	Amorphous	-
	500	Amorphous	-
	525	Amorphous	-
	540	Amorphous	-
	570	α-Fe(Si)	6
	600	α-Fe(Si)	15
17.5	As cast	Amorphous	-
	500	Amorphous	-
	525	Amorphous	-
	540	Amorphous	-
	570	α-Fe(Si)	4
	600	α-Fe(Si)	14

The maximum grain size is found to be within the range from 18 nm to 20 nm after annealing at T_a = 600°C, for the sample of low Cr content and from 14 to 15 nm for the samples of increasing amount Cr element, as shown in Table 2. For samples with x = 12.5 and 17.5, a noticeable crystallization begins at T_a = 570°C but remains diffuse, only becoming slightly defined at T_a = 600°C. Therefore, the role of Cr in delaying the crystallization of the amorphous $Fe_{73.5-x}Cr_xCu_1Nb_3Si_{13.5}B_9$ system during thermal treatment around the first crystallization temperature is clearly interpreted from a detailed analysis of the XRD spectra.

In the case of Fe-based nanocrystalline alloys $Fe_{73.5-x}Cr_xCu_1Nb_3Si_{13.5}B_9$ the increase in grain size largely depends on the amount of element Cr and annealing temperature. Small amount Cr (*e.g.*, x=1) acts as a grain growth inhibitor due to its atomic structure and the pinning effect, where it tends to restricts the movement of grain boundaries. However, when increasing amount of Cr is added (*e.g.*, x=12.5 or x=17.5) its inhibiting effect starts to diminish, allowing grains to grow more freely. The addition of Cr at higher concentrations can also reduce the stability of the amorphous phase and alter the free energy landscape, leading to a faster nucleation rate and growth of grains at higher temperatures. The grain boundary mobility also tends to increase with addition of more Cr, facilitating quicker growth as annealing temperature rises. Annealing at higher temperatures generally provides sufficient energy for atomic diffusion, which is necessary for grain boundary migration and growth. For x = 12.5 or x = 17.5, the grain size increases more dramatically (e.g., from 4 to 14 nm or from 6 to 16 nm) between 570 K and 600 K, showing that the thermal activation energy is more readily utilized for grain growth due to the lessened in hibition effect with higher Cr content. Thus, we may conclude that for higher Cr content the grain growth becomes more pronounced at elevated temperatures.

3.3 Microstructural study of $Fe_{73.5-x}Cr_xNb_3Cu_1Si_{13.5}B_9$ by FESEM

Figure 3 (a-d) exhibits the microstructure of sample Cr = 1 after heat treatment at diverse annealing temperatures (T_a = 480°C, 520°C, and 550°C), alongside the sample in as-cast condition. For the sample in as-cast state (Figure 3(a)) no appearance of crystallization is observed with a clear amorphous background. This behavior is consistent across every other sample in as-cast state. The process of crystallization starts to develop with increasing annealing temperature. In Figure 3(b), in case of sample alloy for x = 1 at T_a = 480°C no distinct grains are observed, but a cluster-like agglomerate is clearly visible, which can be described as the phase immediately preceding to the start of crystallization. Figure 3(c) depicted the microstructure of the sample annealed at temperature T_a=520°C, where crystallization has begun, and nanograins have started to form. However, these nanograins are still far apart and tend to clustered together. When the sample is annealed at T_a=550°C (Figure 3(d)), complete crystallization is observed, with a large number of closely spaced nanograins. Despite this, the nanograins remain clustered together.

The sizes of the grains are calculated from the microstructures appear to be bigger than those are calculated from the data obtained XRD experiment, as shown in Table 2. This difference could be due to the limitations of the XRD technique in detecting agglomerated structures or due to the inherent differences in how grain size is assessed using different methods.

All the samples under the investigation exhibit crystallization events at annealing temperatures near the first peak of crystallization temperature (T_{p1}) ascertained from the DSC thermogram, where we have observed well-defined nanograins. The results obtained from XRD, DSC, and FESEM examination are found to be highly consistent with each other. Figure 4 (a-d) illustrate the microstructure of the sample having Cr content x = 5 in the as-cast state, and also after annealed at temperatures of 500°C, 540°C, and 570°C. Evidently, Figure 5 demonstrate that the crystallization begins at T_a = 540°C, where the grains seem to be highly agglomerated which are spaced far from each other, making it challenging to find out their exact sizes. The crystallization is fully formed by T_a = 570°C, with grain sizes below 25 nm. However, due to agglomeration, the actual grain size cannot be easily observed.

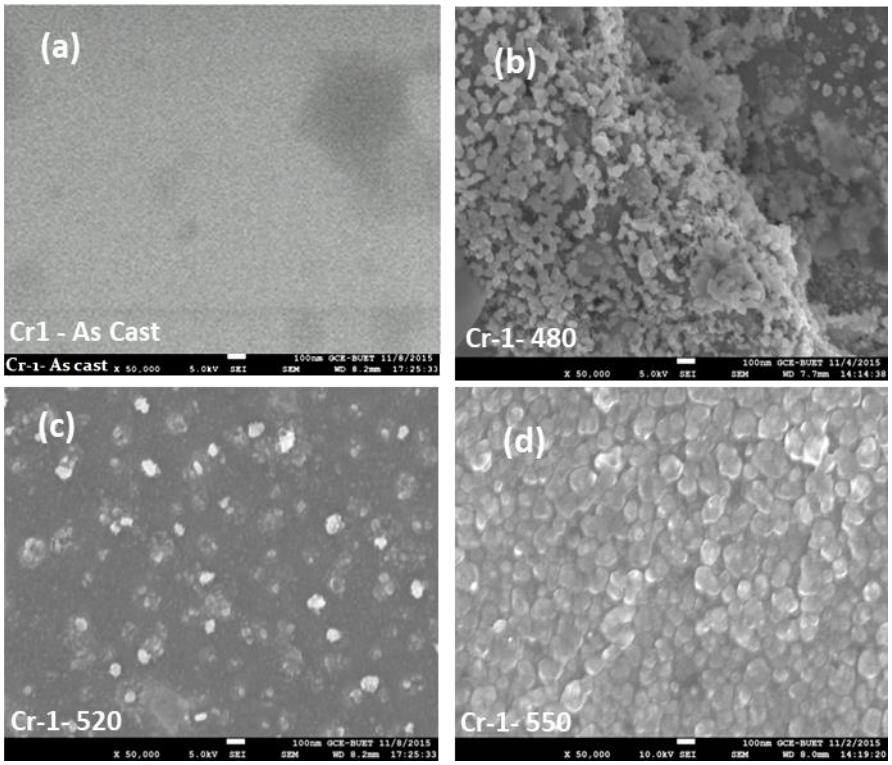

Fig. 3: FESEM microstructure of $Fe_{73.5-x}Cr_xNb_3Cu_1Si_{13.5}B_9$ where x= 1 at (a) as cast and annealed at temperatures (b) 480ºC, (c) 520ºC and (d) 550ºC.

XRD analysis for the sample with Cr content x = 10 grain of size 4 nm is obtained at T_a = 540°C and 12 nm at T_a = 570°C. We see from DSC data (as shown in Table 1) for this sample the crystallization peak temperature is T_{p1} = 544°C, where the onset crystallization temperature, T_{x1} = 514°C. The FESEM, DSC, and XRD results are found to be well-aligned, providing a consistent picture of the crystallization process across the different measurement techniques applied in current study.

Figure 6 (b, c, d) shows the microstructural evolution of the sample with Cr = 12.5 after annealing at temperatures states namely 540°C, 570°C, and 600°C. From the FESEM images, it is evident that crystallization begins at T_a = 540°C, consistent with the DSC data (T_{x1} = 517°C and T_{p1} = 550°C). At T_a = 570°C, agglomerated grains are visible, though still small in size. By T_a = 600°C, well-defined nanometric grains are observed, indicating a more mature crystallization process. These observations are consistent with the XRD data provided in Table 2.

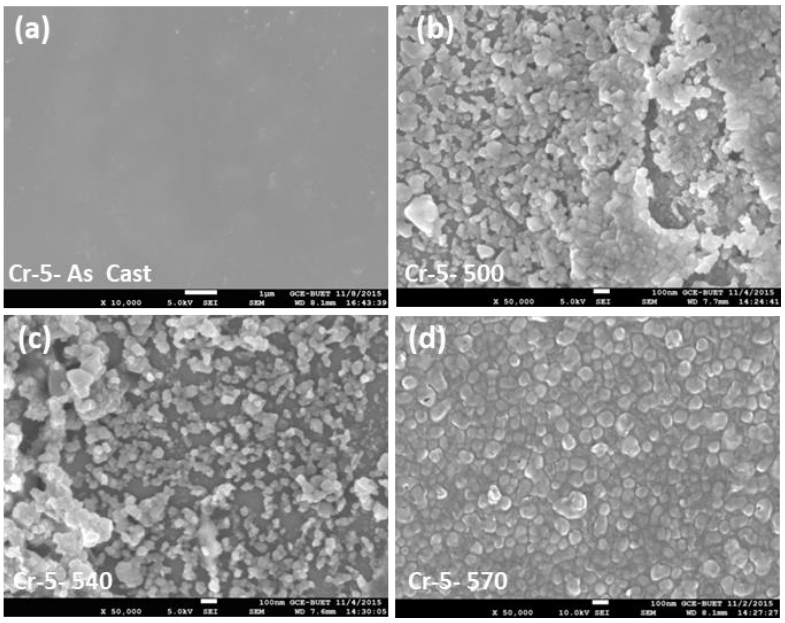

Fig. 4: FESEM microstructure of $Fe_{73.5-x}Cr_xNb_3Cu_1Si_{13.5}B_9$ for x = 5 (a) as cast condition, and at annealing temperatures (b) 500°C, (c) 540°C and (d) 570°C respectively.

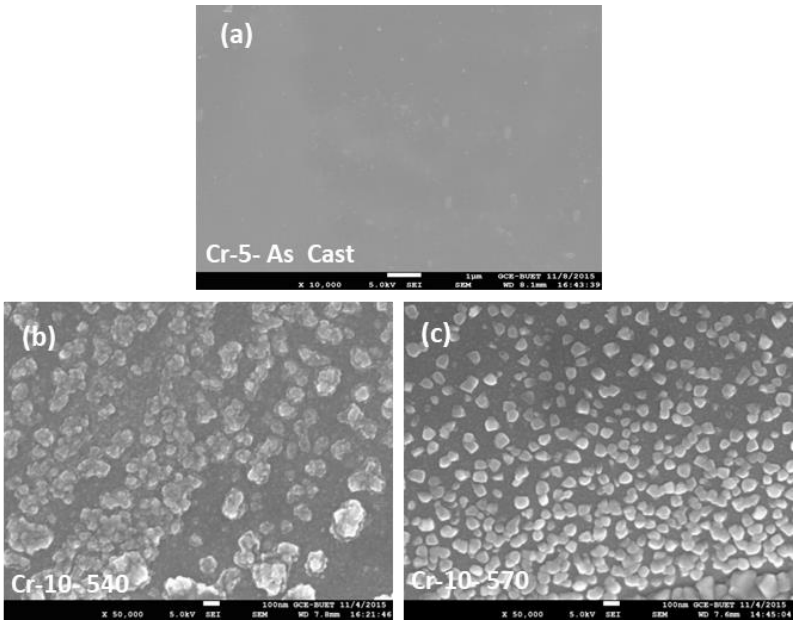

Fig. 5: FESEM microstructure of $Fe_{73.5-x}Cr_xNb_3Cu_1Si_{13.5}B_9$ for x = 10 (a) as cast condition and at annealing temperatures (b) 540°C, and (c) 570°C respectively.

The microstructure obtained from FESEM experiment for sample with Cr = 17.5, is shown in Figure 7 at different annealing temperatures 570°C, 600°C, and 650°C. At T_a = 570°C, small nanograins of size less than 10 nm become visible (Figure 7(b)), with the XRD analysis indicating a grain size of approximately 4 nm. The grain size increases significantly when annealing temperature rises to 600°C (Figure 7(c)), and the sizes match reasonably well with the XRD data, which suggests grain sizes would be around 14 nm.

The FESEM analysis clearly demonstrates that the crystallization behavior of $Fe_{73.5-x}Cr_xCu_1Nb_3Si_{13.5}B_9$ amorphous alloys in the form of 25 μm thick ribbons is strongly influenced by Cr concentration and the annealing temperature. The higher the Cr content, the more difficult it becomes for crystallization to occur, indicating that Cr contributes to the thermal stability of the alloy against crystallization [18]. As Cr content increases, the growth of nanograins is increasingly inhibited, a trend that is consistently reflected across both the XRD data and microstructural images. Finally, we can say that the results from XRD data (Table 2) and the microstructural images obtained for samples with varying Cr content and annealed at different temperatures the increasing of Cr content leads to smaller grain sizes at the same annealing temperature.

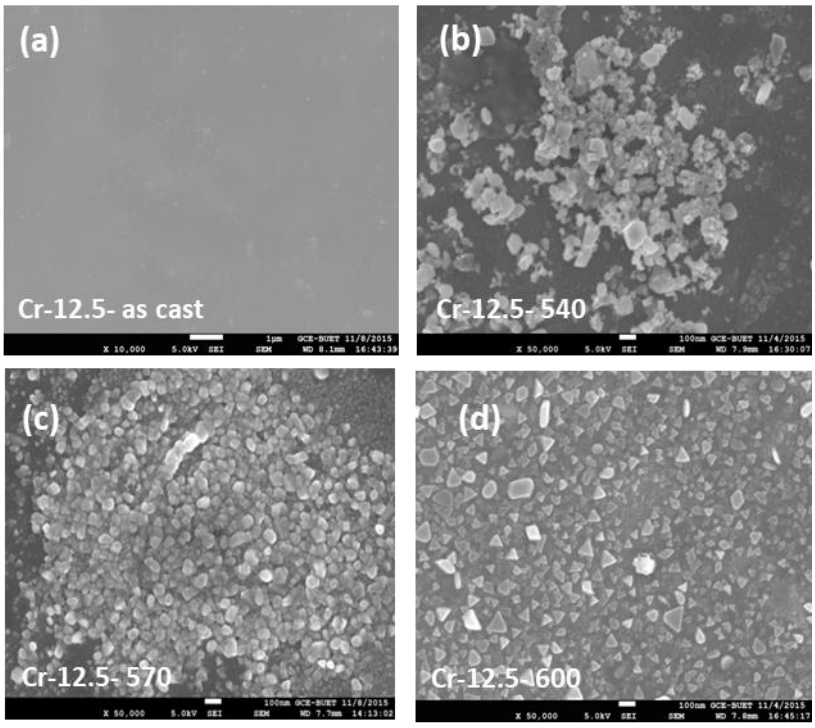

Fig. 6: FESEM microstructure of $Fe_{73.5-x}Cr_xNb_3Cu_1Si_{13.5}B_9$ where x = 12.5 (a) as cast and annealed at temperatures (b) 540ºC, (c) 570ºC and (d)600ºC.

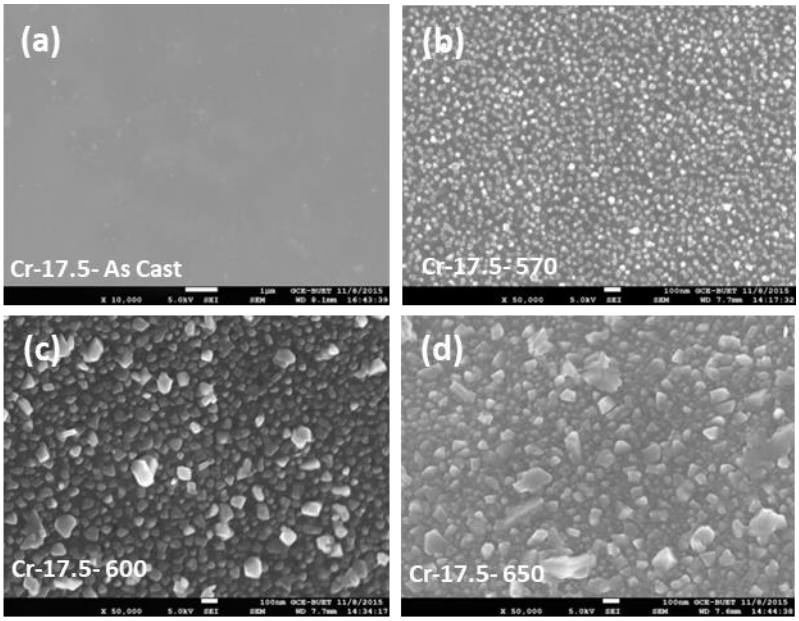

Fig. 7: FESEM microstructure of $Fe_{73.5-x}Cr_xNb_3Cu_1Si_{13.5}B_9$ where x=17.5(a) as cast and annealed at temperatures (b) 570ºC, (c) 600ºC and (d) 650ºC.

4. CONCLUSIONS

This report centered on investigating the effect of varying Cr content and heat treatment behavior on the structural properties of amorphous $Fe_{73.5-x}Cr_xCu_1Nb_3Si_{13.5}B_9$ alloys. The results from Differential Scanning Calorimetry (DSC), X-ray Diffraction (XRD), and Field Emission Scanning Electron Microscopy (FESEM) demonstrated that the crystallization process is greatly affected by both Cr concentration and annealing temperature. The introduction of Cr into the alloy system increases its thermal stability, delaying the onset of crystallization. Higher Cr content results in a more sluggish crystallization process, leading to finer grain sizes, particularly at elevated annealing temperatures. For lower Cr content samples, the crystallization process begins at lower temperatures, and larger nanograins are formed. The study confirms that Cr addition enhances the thermal stability of the Fe-Si-B based alloys, making them promising candidates for applications requiring soft magnetic materials with fine-grained structures. Future research could explore further optimization of Cr content to fine-tune the magnetic and mechanical properties of such alloys for industrial applications.

REFERENCES

[1] J. Petzold, Journal of Magnetism and Magnetic Materials **242** (2002) 242–245.

[2] T. H. Kim, K. K. Jee, Yoon B. Kim, D. J. Byun, J.H. Han, Journal of Magnetism and Magnetic Materials, **322** (2010) 2423–2427.

[3] Kazi Hanium Maria, Saadni Islam, Shamima Choudhury, Mohammad Abdul Hakim, Dilip Kumar Saha, Shiekh Manjura Hoque, Int. Nano Lett., **1** (2011) 97-102.

[4] Siba Pada Mondal, M. Mahbubur Rahman, S. S. Sikder and M. A. Hakim, Journal of Eneineerins Science, **02** (2010) 59-64

[5] Zhang, Y. R., and R. V. Ramanujan, Materials Science and Engineering: A, **416**, (2006) 161-168.

[6] M. A. Hakim, S. Manjura Hoque, M. Khalilur Rahman, Jamal Uddin Ahamed, Journal of Nuclear Science and Applications, **14**, (2005) 35-40.

[7] Bayri, N., T. Izgi, H. Gencer, P. Sovak, M. Gunes, and S. Atalay, Journal of Non-Crystalline Solids, **355** (2009) 12-16.

[8] Song, Yiming, Min Jia, Min Lin, Xiang Li, and Wei Lu, Journal of Alloys and Compounds, **622** (2015) 500-503.

[9] Verduzco, J. A., I. Betancourt, F. Saavedra, and E. Reynoso, Journal of Non-Crystalline Solids, **329** (2003) 163-166.

[10] Enayet Hossain, Shamima Choudhury, M. A. Bhuiyan, K. H. Maria, M. H. Mesbah Ahmed, D. K. Saha, and M. A. Hakim, Advanced Science Focus, **2**, (2014) 12–16.

[11] Sharma, Pooja, and Ajay Gupta, Nuclear Instruments and Methods in Physics Research Section B: Beam Interactions with Materials and Atoms, **244** (2006) 105-109.

[12] Crisan, O., J. M. Le Breton, and G. Filoti, Sensors and Actuators A: Physical, **106** (2003) 246-250.

[13] Islam, Saadni, Kazi Hanium Maria, Shamima Choudhury, Turkish Journal of Physics, **36** (2012) 253-259.

[14] Millán, M., C. F. Conde, and A. Conde, Journal of Materials Science, **30** (1995) 3591-3597.

[15] Jörg F. Löffler, Intermetallics, **11 (**2003) 529-540.

[16] Mahmud, Md Sultan, Asian Transactions on Science & Technology, **01** (2011) 1-6.

[17] Zhang, Changqin, Zhengwang Zhu, and Haifeng Zhang, Journal of Physics and Chemistry of Solids **110** (2017) 152-160.

[18] Han, Jia-jia, Cui-ping Wang, Sheng-zhong Kou, and Xing-jun Liu, Transactions of Nonferrous Metals Society of China, **23** (2013) 148-155.